THE JOURNAL OF PHYSICAL CHEMISTRY B

ARTICLE

pubs.acs.org/JPCB

Proton Solvation and Transport in Hydrated Nafion

Shulu Feng and Gregory A. Voth*

Department of Chemistry, James Franck Institute and Computational Institute, University of Chicago, 5735 S Ellis Ave., Chicago, Illinois 60637, United States

ABSTRACT: Proton solvation properties and transport mechanisms have been studied in hydrated Nafion using the self-consistent multistate empirical valence bond (SCI-MS-EVB) method that includes the effects excess proton charge defect delocalization and Grotthuss proton hopping. It was found that sulfonate groups influence excess proton solvation, as well as the proton hydration structure, by stabilizing a more Zundel-like ($H_5O_2^+$) structure in their first solvation shells. Hydrate proton-related hydrogen bond networks were observed to be more stable than networks with water alone. Diffusion rates, Arrhenius activation energies, and transport pathways were calculated and analyzed to characterize the nature of the proton transport. Diffusion rate analysis suggests that a proton-hopping mechanism dominates the proton transport for the studied water loading levels and that there is a clear degree of anticorrelation with the vehicular transport. The activation energy drops quickly with an increasing water content when the water loading level is smaller than ~10 H_2O/SO_3^-, which is consistent with experimental observations. The sulfonate groups were also found to affect the proton hopping directions. The temperature and water content effects on the proton transport pathways were also investigated.

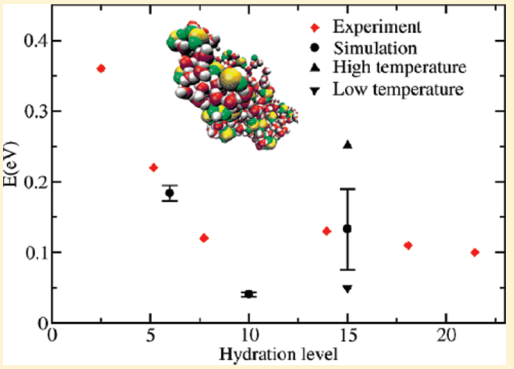

1. INTRODUCTION

Perfluorosulfonic acid (PFSA) polymer membrane is the principal electrolyte and separator adopted in polymer electrolyte membrane fuel cell (PEMFC) technology, which is the state-of-the-art method in producing and delivering energy. PFSA membranes exhibit good properties for fuel cell incorporation, such as reasonably high proton transport (PT) rates and mechanical elongation, low permeability for both oxygen and hydrogen,[1] and high chemical stability in reducing and oxidizing environments.[2] However, PFSA membranes also suffer from having a narrowly defined operational temperature, carbon monoxide poisoning, and methanol crossover issues[1−3] in their practical use. Many research efforts have been focused on eliminating the above barriers by synthesizing new electrolyte polymers to substitute for PFSA[4] or by modifying the existing polymers.[5−7] Of all the PEMFC-related issues, the key discussion revolves around how protons transport through the polymer electrolyte membrane. Obtaining a thorough understanding of proton solvation structure and the transport mechanisms is therefore of critical importance.

Among all of the PFSA membranes, Nafion generally receives the most attention due to its general degree of availability.[8] Substantive experiments have been employed to investigate the PT mechanism in Nafion. The proton-hopping mechanism, that is, the Grotthuss mechanism,[9−15] was shown to explain successfully some experimental results regarding the PT in Nafion.[16,17] However, the details of the proton-hopping mechanism are still debated given the complexity of the material and of the PT process itself.[15] The Nafion structure and side-chain effects on the PT and excess proton solvation introduce more challenges to a thorough understanding of the PT mechanism in Nafion. It has also been found that the transport mechanism is strongly related to water concentration. For example, Ochi et al. have analyzed the diffusion coefficients using NMR and electrical conductivity measurements.[16] D'Epifanio et al. compared the proton diffusivity and water diffusivity, determining that the difference becomes significant only at high humidification (hydration) levels.[18]

Theoretical and computational studies have been extensively employed to study the PT problem in PFSA polymer membranes.[7,19−39] Most of these studies utilize classical hydronium cation models (i.e., models that do not incorporate excess proton charge defect delocalization and Grotthuss hopping) and so any apparent agreement with experimental results in those simulations is at least partly accidental. Computational models have also been proposed and simulated to explore the morphology of Nafion.[23,27,40−43] Additionally, extra-large scale atomistic molecular dynamics simulations with different proposed models have been run to study the morphology of Nafion.[43]

The side chains of Nafion, which contribute to the hydrophilic domain, are considered to be an important factor influencing the PT; these side chain effects have received much study.[19,20,25,37] The effective friction coefficient of a hydrated proton increases quickly when approaching the fixed sulfonic acid site.[20] Nafion was furthermore found to have the most mobile side chains at a water loading level of 15.[25] The proton hopping activation energy along a surface with charged sulfonic groups increases

Received: January 8, 2011
Revised: April 3, 2011
Published: April 21, 2011

with the average distance between the sulfonic groups.[19] Karo et al. reported the side chain length effects in the two well-known PFSAs (Nafion and Hyflon) and found that the water and hydronium ion have a higher diffusion coefficient in the Hyflon due to the shorter side chain.[37] They also found that Nafion shows a higher degree of phase segregation than Hyflon due to the longer side chain.

The PT mechanisms have also been investigated, despite the fact that the details of the Nafion structure are unclear. The Grotthuss hopping mechanism was suggested to be the dominant mechanism for Nafion transport with a water loading level between 5 and 10.[23] It was further suggested that the Zundel cation, $H_5O_2^+$, is the main formation of charge carriers under low water concentration while the Eigen cation, $H_9O_4^+$, begins to form as the water concentration increases.[26] However, these early studies utilized a fairly limited proton transport simulation methodology. A subsequent study[24] utilizing a more physically complete proton solvation and transport modeling,[44] that is, one that includes the various possible features of the excess proton charge defect delocalization and Grotthuss hopping, found that the vehicular and hopping mechanisms both contribute to the PT and can be to some degree negatively correlated.[24]

The latter studies on PT in hydrated Nafion[24] also explored the characteristics of sulfonate-hydrated proton ion pairs as well as vehicular motion and the proton hopping contribution to the proton diffusion. In the present work, Nafion/water mixtures with even lower water content and at higher temperatures have been simulated to provide a more in-depth interpretation of the proton solvation structure, as well as the PT mechanism. These results build significantly on the work of ref 24.

This article is organized as follows: the simulation setup is discussed in section 2, whereas the simulation results are discussed in section 3. Conclusions are then drawn in section 4.

2. METHODS

The self-consistent multistate empirical valence bond (SCI-MS-EVB) methodology[44] has been used in this work to characterize the intrinsic nature of the hydrated excess protons at high concentration. As an extension of the MS-EVB method,[45,46] the SCI-MS-EVB method has the ability to capture the underlying physics of multiproton systems with a computational efficiency that scales linearly with the number of protons. In this work, the newly developed MS-EVB3 parameters[47] were employed, which also includes a more accurate underlying flexible water model.[48] The Nafion force field from Jang et al.,[40] which was utilized in our previous study,[24] was used in the present work with the hydrated protons treated by the SCI-MS-EVB method.

Nafion systems with water loading levels of 6, 10, and 15 molecules per sulfonic acid group (referred as hydration levels 6, 10, and 15) were constructed at 298, 320, and 340 K. Four Nafion chains with equivalent molecular weight ~1100 were randomly distributed in the simulation box. Each one contained 10 sulfonate groups. The corresponding numbers of water molecules were then added for different hydration levels. All of the systems were first equilibrated by the Gromacs[49] molecular dynamics package using the classical hydronium model to present the excess protonic charges. Subsequently, constant NPT simulations of 8 ns were utilized to relax the system to the desired pressure of 1 atm. Constant NVT simulations of 12 ns were then employed to equilibrate the system further.

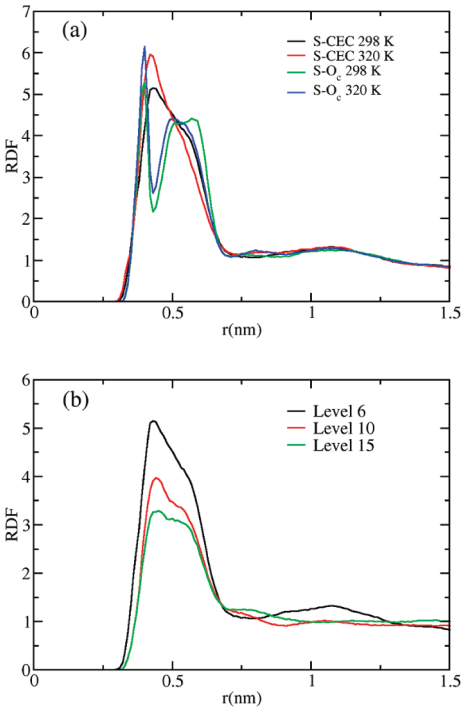

Figure 1. (a) Radial distribution functions (RDFs) of hydration level 6: sulfur atom of the Nafion side chain (S) and proton center of excess charge (CEC) at 298 K (black line), S and CEC at 320 K (red line), S and oxygen atoms with the largest EVB amplitude (O_c) at 298 K (green line), S and O_c at 320 K (blue line); (b) RDFs of CEC and S at 298 K: hydration level 6 (black line), hydration level 10 (red line), hydration level 15 (green line).

The equilibrated structures from the constant NVT simulations with the classical hydronium model were then adopted as the initial structures in the SCI-MS-EVB simulations, with the MS-EVB3 potential turned on. For each system, a 200 ps simulation in the constant NVT ensemble was employed to relax the structures under the full MS-EVB3 potential. The final structures for each system were then used as the initial structures for constant NVE simulations with a cutoff of 10 Å and the Ewald summation for calculating all of the electrostatic interactions. A total of 1 ns simulation data for hydration levels 6, 10, and 15 and initial temperatures at 298, 320, and 340 K respectively were collected with a data collection interval of 100 fs.

The center of excess charge (CEC) that characterizes the instantaneous location of the center of the delocalized excess proton charge defect and most physically accurately describes the effects of Grotthuss proton shuttling was used to describe the hydrated excess protons. The position of the CEC ($\vec{r}_{CEC}$) is calculated by the following two functions:[24]

$$\overrightarrow{CEC}_i = \left[\frac{\sum_{j}^{\text{atoms}(H_3O^+)} |q|_{j;i}\, \vec{r}_{j;i}}{\sum_{j}^{\text{atoms}(H_3O^+)} |q|_{j;i}} \right] \quad (1)$$

$$\vec{r}_{CEC} = \sum_{i}^{\text{states}} c_i^2 (\overrightarrow{CEC}_i) \quad (2)$$

dx.doi.org/10.1021/jp2002194 |J. Phys. Chem. B 2011, 115, 5903–5912

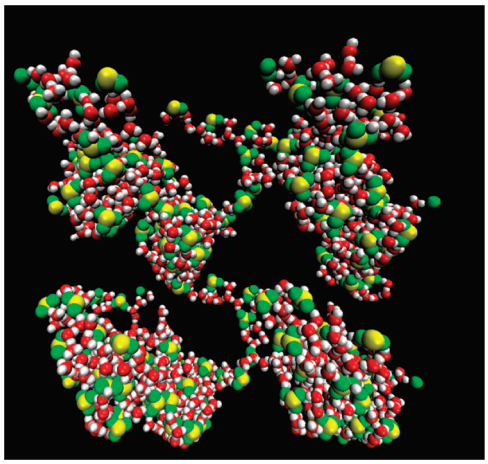

Figure 2. Typical hydrophilic domains of the simulated system with hydration level 6 at 298 K (the simulation box was duplicated in two dimensions to give a better visual description): sulfur atoms in the sulfonate groups (yellow spheres), oxygen atoms in the sulfonate groups (green spheres), oxygen atoms in water (red spheres), hydrogen atom in water and excess protons (white spheres).

Wherein $CEC_i\rightarrow$ is the position of the CEC in the ith MS-EVB state; $|q|_{j;i}$ represents the charge on atom j in the ith state; $\vec{r}_{j;i}$ is the position of atom j in the ith state; c_i^2 is the amplitude of the ith states in the MS-EVB complex. The oxygen atom with the largest MS-EVB amplitude c_i^2 is also useful to describe the PT behavior. These atoms are the closest oxygen atoms to CECs and are referred to as O_c.

3. RESULTS AND DISCUSSION

3.1. Proton Solvation. *3.1.1. Proton Distributions.* The proton solvation structure is influenced by the nearby environment.[24] Therefore, the excess proton distribution is analyzed first. In Figure 1, the radial distribution functions (RDFs) of sulfur atoms and other particles are shown. The RDFs between sulfur and the most hydronium like oxygen O_c, show a strong narrow peak at 4 Å with the first minimum at ~4.3 Å. Thus, 4.3 Å is used to define the first solvation shell of sulfonate groups. Interestingly, the RDFs between the sulfur atom and the CEC show a wide peak around 4.3 Å. The wide peak of S-CEC is the reflection of the delocalization nature of the proton charge defects.

Before further exploring the proton distribution around the sulfonate groups, it is helpful to examine the distribution of sulfonate groups first. One snapshot taken from the simulation is shown in Figure 2. Sulfonate groups gather together to form hydrophilic domains. The first solvation shells of some sulfonate groups even overlap, and water and excess protons are inside the domains. Similar results were also reported in several other computational studies.[21,43]

It should be noted that as the temperature increases from 298 to 320 K, more excess protons reside closer to the sulfonate groups (part a of Figure 1). Similarly, several simulations with classical hydronium cation models found that more hydronium ions are around the sulfonate groups with an increase of temperature.[31,39] In the present simulations, it was found that the distribution difference at different temperature is strongly correlated with the proton solvation structure, which is discussed in section 3.1.2. When the hydration level increases from 6 to 15 (part b of Figure 1), the intensity of the first peaks decreases as expected, indicating fewer excess protons around the sulfonate groups, due to the increased content of water molecules.

3.1.2. Proton Solvation Structure at Different Hydration Levels and Temperatures. Our previous study revealed that the excess proton is mostly solvated in the form of Zundel-like cations when in close contact with sulfonate groups.[24] To further investigate the proton solvation properties, the first two largest MS-EVB amplitudes (c_1^2 and c_2^2) were used to characterize the solvation structure of protons. The distributions of the difference $\Delta c^2 = c_1^2 - c_2^2$ are depicted in Figure 3. A difference around 0 corresponds to the Zundel-like solvation structure, while a difference larger than ~0.4 corresponds to the Eigen-like structure. The excess protons have been divided into two groups: the first group (G1) contains the proton in the first solvation shell of sulfonate groups, whereas the other (G2) contains the rest. The distributions of Δc^2 for the two groups are calculated separately. The distribution is scaled so that the relative amplitude corresponds to the relative number of protons. As shown in Figure 3, when comparing the protons in G1 to those in G2, more protons in G1 prefer a Zundel-like cation solvation structures in the given temperature and water content range.

The above results indicate that the sulfonate groups can stabilize the Zundel-like cations. Further insight may be gained by analyzing their structure in the neighborhood of the sulfonate groups. The RDF results of oxygen atoms in the sulfonate groups with the hydrogen atoms shows a peak at around 1.7 Å, (part d of Figure 3), which is shorter than the length of typical water hydrogen bonds. These stronger hydrogen bonds contribute to stabilizing the Zundel-like cations in the first solvation shell.

As the temperature increases, more excess protons in the G1 group have Zundel-like solvation structures. When considering the RDF results in section 3.1.1, the increase of the peak at around 4.3 Å is due to more excess protons with Zundel-like solvation structure present around the sulfonate groups. As the temperature increases, water molecules move away from the sulfonate groups, resulting in reduced screening effects.[39] Therefore, the effective electrostatic interactions between the sulfonate groups and the hydrated excess protons that are not in close contact is increased, leading to more protons around the sulfonate groups.

A comparison of the excess proton distribution at different hydration levels is shown in part c of Figure 3. As the hydration level increases from 6 to 15, the reduced intensity of the distribution represents the decrease of protons in the first solvation shell. The distribution of different proton solvation structures also changes. From part c of Figure 3, as the water loading level increases from 6 to 10, more excess protons are found in the Eigen-like solvation structure beyond the first solvation shell of the sulfonate groups. A further increase in the hydration level from 10 to 15 shows the number of protons in the Eigen and Zundel-like solvation structures decreasing at a similar rate. This indicates that the sulfonate groups' influence on proton solvation is significantly weakened when the hydration level increases beyond 10.

3.1.3. Proton Solvation Structure Stability. The stability of the excess proton solvation structure was analyzed based on the hydrogen bonding network. Several specific O−O−H types of angles are defined in the insert of Figure 4 (α_1, α_2, α_3, β_1, and β_2). When the distance between two oxygen atoms is smaller than 3.5 Å, the angle is calculated. The distribution of the calculated results is depicted in Figure 4. The area with angle <30° usually corresponds to the formation of hydrogen bonds.

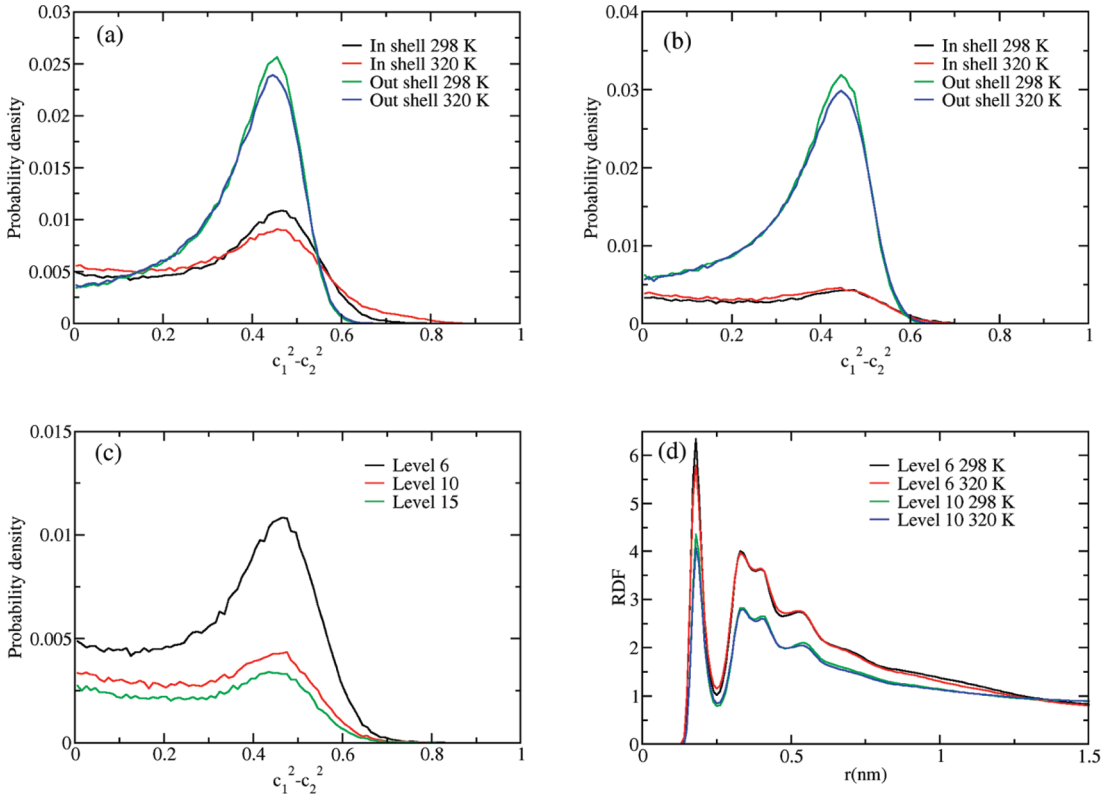

Figure 3. Distribution of MS-EVB coefficient difference $\Delta c^2 = c_1^2 - c_2^2$ for hydrated protons in the system with (a) hydration level 6 and (b) level 10. Black line, protons in the first solvation shell of sulfonate groups at 298 K; red line, protons in the first solvation shell at 320 K; green line, protons out the first solvation shell at 298 K; blue line: protons out the first solvation shell at 320 K. (c) The distribution of $c_1^2 - c_2^2$ for protons in first solvation shell at 298 K with hydration level 6 (black line), 10 (red line), and 15 (green line). (d) RDFs of oxygen atoms in the sulfonate groups and all the hydrogen atoms at hydration level 6 and 298 K (black line), hydration level 6 and 320 K (red line), hydration 10 and 298 K (green line), hydration 10 and 320 K (blue line).

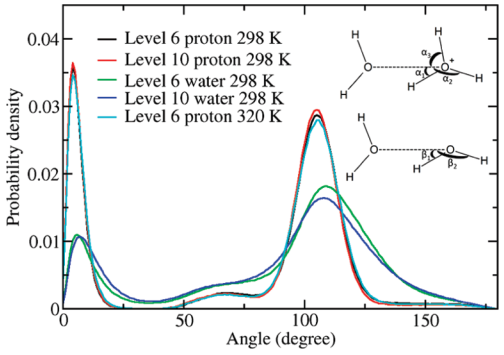

Figure 4. Distribution of angle O−O−H (α_1, α_2, α_3, β_1, and β_2) defined in the insert. Black line, proton-related angles (including α_1, α_2 and α_3) at hydration level 6 and 298 K; red line, proton-related angles at hydration level 10 and 298 K; green line, water-related angles (including β_1 and β_2) at hydration level 6 and 298 K; blue line, water-related angles at hydration level 6 and 298 K; cyan line, proton-related angles at hydration level 6 and 320 K.

The value around 100° contains the contribution from the angle involving the other hydrogen atom connected with the donor. It also includes the angles involving the two close oxygen atoms without a hydrogen bonding connection. Therefore, the peak around 100° is wider than the peak <30°.

For the angle distribution of the water network, the two peaks around 6° and 108° indicate the formation of a water-hydrogen bond network. For the angle distribution of excess proton-related waters (water molecules with significant hydronium character due to an associated excess proton), the two stronger peaks around 4.5° and 105° indicate the formation of a more ordered (and thus likely more stable) hydrogen bond network than for bulk water. With the increase of hydration level, the angle distribution is nearly unchanged, which is another sign of the stability of the proton solvation structures. Similarly, increasing the temperature from 298 to 320 K leads to a very small change in the angle distribution for the proton-related hydrogen-bonding network (as depicted by the cyan curve in Figure 4).

3.2. Proton Transport. *3.2.1. Diffusion.* To characterize the transport behavior of excess protons and the corresponding hydration and temperature effects, the mean square displacements (MSDs) of the CECs were calculated (depicted in part a of Figure 5) with the diffusion coefficients estimated by the MSD slope from 50 to 600 ps, shown in parts b (298 K) and c (340 K) of Figure 5. Experimental measurements[16] at temperatures of 304 and 339.2 K are also plotted in Figure 5. Within the studied water concentration and temperature ranges, proton diffusion rates increase quickly as the hydration level and temperature increase. When the hydration level increases from 6 to 15, the diffusion coefficients increase more than an order of magnitude at 298 K (from $0.014 \pm 0.0044 \times 10^{-4}$ to $0.17 \pm 0.027 \times 10^{-4}$ cm^2/s). At hydration level 6, the diffusion coefficient increases to $0.16 \pm 0.018 \times 10^{-4}$ cm^2/s as the temperature increases to 340 K. The simulation results were found to be in rather close agreement with experimental measurements[16] at the

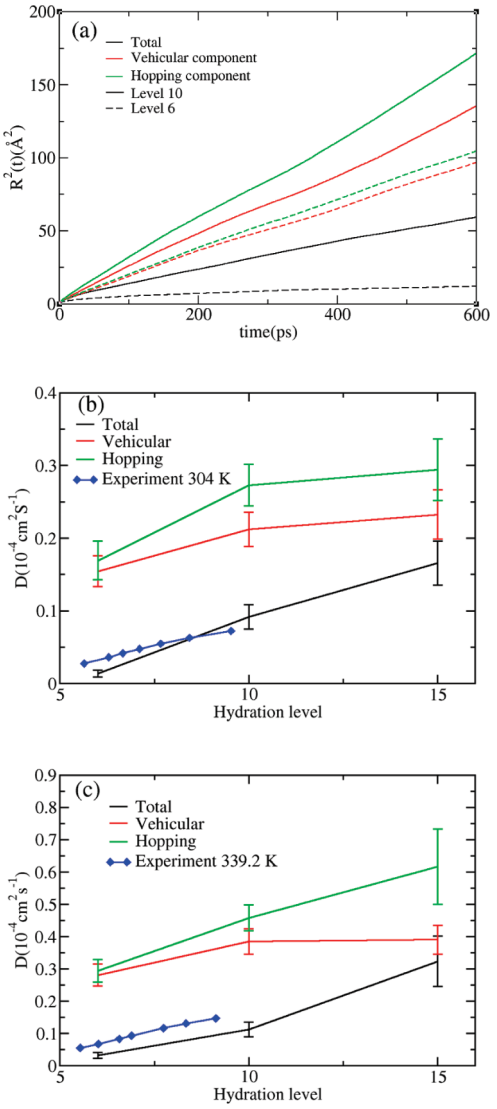

Figure 5. (a) Mean square displacements (MSDs) of CECs at 298 K. Dashed line, hydration level 6; solid line, hydration level 10; black line, total MSD; red line, continuous (vehicular) component; green line, discrete (hopping) component. (b) Diffusion coefficients of CECs at 298 K and experimental results at 304 K. (c) Diffusion coefficients of CECs at 340 K and experimental results at 339.2 K. In (b) and (c): black line, total diffusion coefficients; red line, vehicular diffusion coefficients; green line, hopping diffusion coefficients; blue line with filled square diamond, experimental diffusion coefficients. Error bars were estimated by the bootstrapping technique.

lower temperatures. At higher temperatures, the simulation results were somewhat smaller than the experimental results.

The PT involves both vehicular and hopping motions of the excess protons. Peterson and Voth have analyzed the PT by decomposing the vehicular and discrete (hopping) contributions.[24] The same approach was used here to gain further insight into the hydration and temperature effects on the PT (as depicted in part a of Figure 5). The small total MSD relative to the vehicular and discrete components reveals the anticorrelated nature of proton hopping and vehicular motion.[24] Experimental results have suggested that the proton hopping mechanism becomes more important at higher hydration levels.[16,18] Indeed, from the simulations the MSDs of proton hopping motion are

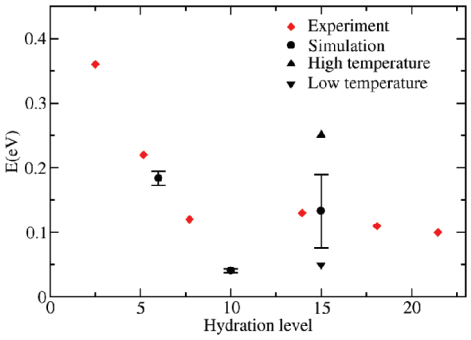

Figure 6. Activation energies at different hydration levels. Red square diamond, experimental results; black circle, simulation results; black triangle up, result calculated from the data at the two highest temperatures; black triangle down, result calculated from the two lowest temperatures. Error bars were calculated based on the average diffusion coefficients.

larger and increase faster than those of the vehicular motion as hydration levels increase from level 6 to 10, as shown in part a of Figure 5. Therefore, the simulation results also indicate that the proton hopping mechanism becomes more significant at higher hydration levels. At the lowest simulated hydration level of 6, the diffusion coefficient of the hopping motion is slightly higher than that of the vehicular motion, indicating that the proton hopping mechanism dominates the PT at hydration levels as low as 6.

When raising the temperature from 298 to 340 K, the diffusion coefficients of the proton hopping motion increase more rapidly than that of vehicular motion, as shown in the red and blue line of parts b and c of Figure 5. Therefore, the temperature plays a similar role to that of water content in altering the PT process.

3.2.2. Activation Energy. The activation energies were calculated for the PT for hydration levels 6 to 15 (depicted in Figure 6). The corresponding Arrhenius plots are shown in Figure 7. Because the Arrhenius plot for level 15 is not linear (part a of Figure 7), the activation energies were also calculated by using the data from the two highest and two lowest temperatures, respectively. Experimental results from impedance spectroscopy[17] are plotted in the same figure for comparison. With an increase of the hydration level, the activation energies can be divided into two regions separated by hydration level 10. Both experimental and simulation results show a sharp decrease of the activation energy with an increase of hydration around the region of hydration level <10. However, the simulation results show an unusually low dip in the activation energy for hydration level 10. This behavior in the simulation seems to be because the hydrophilic domain structure in hydration level 10 is different from the ones in hydration levels 6 and 15. In each simulation box, the hydrophilic part mainly consists of a single large hydrophilic domain at hydration levels 6 and 15. At hydration level 10, the hydrophilic part exhibits a more complicated structure, which can be seen as consisting of several well connected hydrophilic domains. Therefore, the PT in level 10 is more restrained by the sizes and shapes of hydrophilic domains than the PT in levels 6 and 15. When temperature increases, the enhancement of diffusion rates is inhibited by the sizes and shapes of the hydrophilic domains, resulting in the lower activation energy at level 10, even though the diffusion rate is higher than at hydration level 6 (Figure 5).

At high water-loading levels, the activation energies are slightly higher than the activation energy of PT in pure water, which is

dx.doi.org/10.1021/jp2002194 |J. Phys. Chem. B 2011, 115, 5903–5912

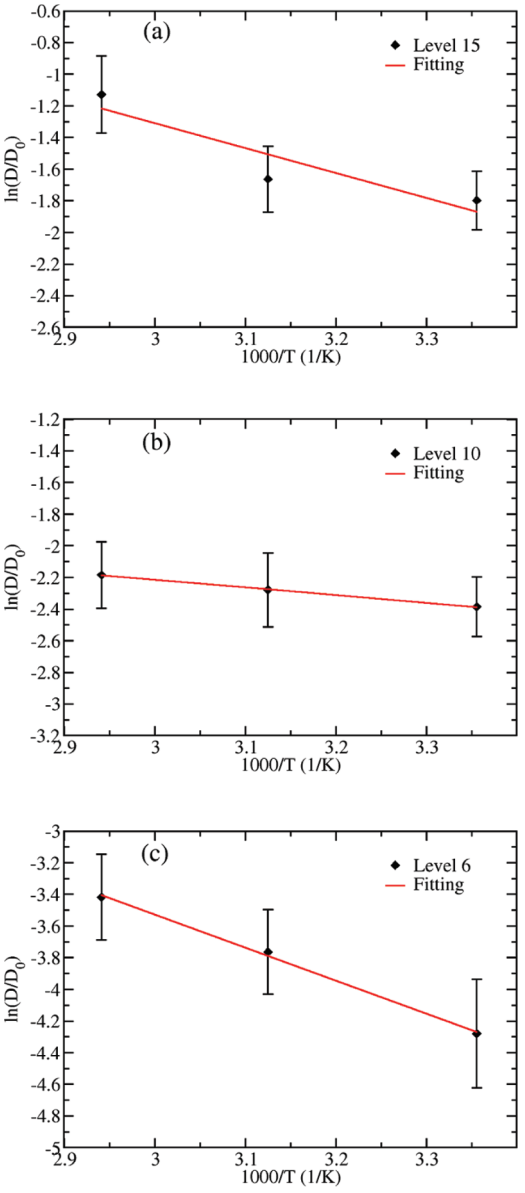

Figure 7. The Arrhenius plots at different hydration levels. D, diffusion coefficient; D_0, constant with value 10^{-4}cm^{2}s^{-1}; T, temperature; black square diamond, simulation data; red line, linear fitting curve.

0.108 eV.[50] The activation energy at high hydration levels may reflect the strength of the hydrogen bonds between bulk water molecules, as Lapid et al. suggested for the activation energy of PT in pure water.[51]

3.2.3. Proton Transport Pathway. (a). Proton Hopping Direction. The PT pathways were analyzed in detail to provide a physical picture of the PT process, with a focus is on how the sulfonate groups influence the PT. The proton hopping direction was calculated as a function of the distance to the closest sulfonate group. Hopping toward the sulfonate group is defined as "backward hopping", while any other movement is defined as "forward hopping". To quantify the forward hopping and backward hopping, a ratio $P(r)$ is defined as:

$$P(r) = \frac{N_b(r)}{N_f(r) + N_b(r)} \quad (3)$$

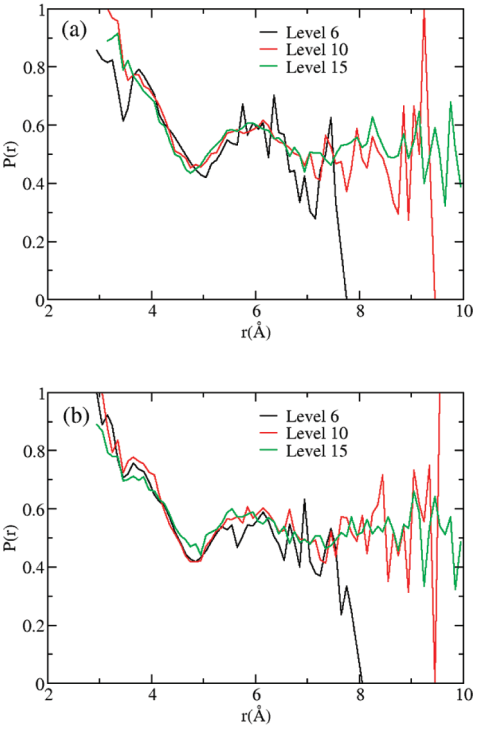

Figure 8. Hopping direction ratio $P(r)$ at 298 K (a) and 320 K (b). Black line, hydration level 6; red line, hydration level 10; green line, hydration level 15.

Wherein $N_f(r)$ is the number of occurrences of forward hopping, $N_b(r)$ is the number of occurrences of backward hopping, and r is the shortest distance between the excess proton CEC and the sulfur atoms in the sulfonate groups.

The results of $P(r)$ show an interesting minimum at $r_m \approx 5$ Å (depicted in Figure 8). The r_m divides $P(r)$ into two regions. When $r < r_m$, more protons hop to the sulfonate groups as r decreases as one might expect. As $r > r_m$, the ratio $P(r)$ fluctuates around 0.5. Within the studied temperature and hydration level range, the value of r_m does not change to any great degree.

Another distance of interest is 4.3 Å, which is also the distance used to define the sulfonate groups' first solvation shell. At this point, the ratio $P(r)$ approaches 0.5 for the first time. Therefore, the proton hopping direction is significantly influenced if it is within the first solvation shell of the sulfonate. For all of the studied systems, there is a region in which the frequency of forward hopping is greater than that of backward hopping. In the studied systems, the region is about 4.3 to 5.0 Å. This change in net proton hopping direction may be rationalized by the electrostatic interactions between excess protons and sulfonate groups. For the region within the first solvation shell, the attraction between the protons and the sulfonate group is the dominant factor controlling the proton hopping direction. For the protons in the region of 4.3 to 5 Å, the repulsion with other protons in the first solvation shell becomes more important, resulting in greater occurrence of forward hopping.

(b). Proton Transport Distance. To characterize how the proton transports from one sulfonate group to another, the distribution of PT distances dr is depicted in Figure 9. The quantity dr is defined as the PT distance from leaving the first solvation shell of one sulfonate group to entering the first solvation shell of another sulfonate group. The value of dr is

dx.doi.org/10.1021/jp2002194 |J. Phys. Chem. B 2011, 115, 5903–5912

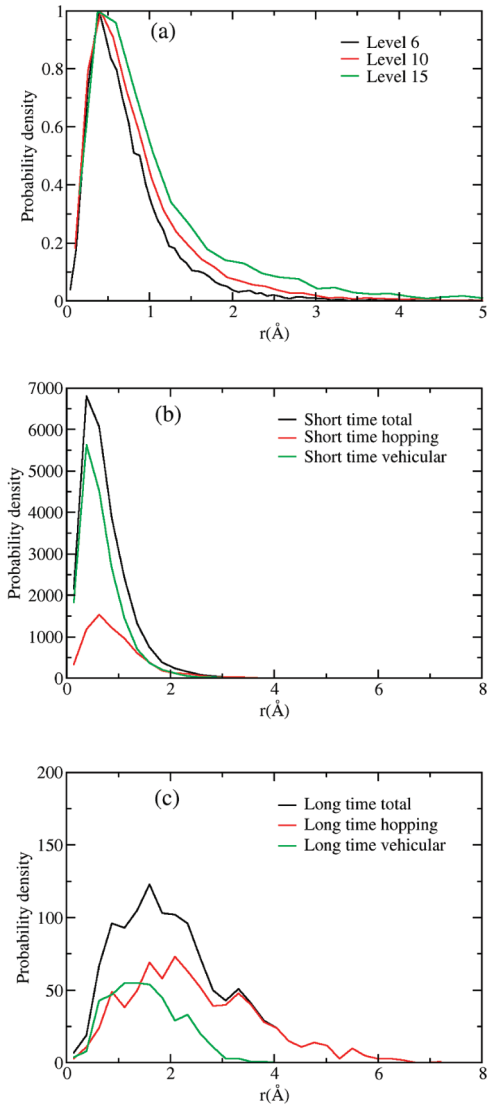

Figure 9. (a) Distribution of the proton transport pathway distance at 298 K. Black line, hydration level 6; red line, hydration level 10; green line, hydration level 15. (b) Distribution of the proton transport pathway distance with transport time <1.27 ps for hydration level 6 at 340 K. Black line, total distribution; red line, hopping component; green line, vehicular component. (c) Distribution of proton transport pathway distance with transport time >1.27 ps for hydration level 6 at 340K. Black line, total distribution; red line, hopping component; green line, vehicular component.

different from the average distance between two sulfonate groups since most protons transfer between the two closest sulfonate groups. Therefore, the average value of *dr* is smaller than the average distance between the sulfonate groups. As shown in part a of Figure 9, with an increase of water content, the distribution shifts to a larger distance due to the sulfonate groups being separated by more water molecules. As the temperature increases, there is no obvious change in the distribution (results not shown). Therefore, the distribution of *dr* is mainly controlled by the distribution of the sulfonate groups.

To further analyze the PT distance distribution, the PT pathway was divided into two groups according to the experimental hopping rate of 0.79 ps^{-1}.[52] One group contains the pathways between two sulfonate groups with a proton transport time <1.27 ps, whereas the other group includes the pathways with a transport time >1.27 ps. Considering the sulfonate groups' distribution discussed in section 3.1.1, the first group mainly represents the type of transport pathway where two sulfonate groups are so proximate that the proton can move easily from one sulfonate group to the other. The first group was further broken down into its hopping and vehicular components (shown in the red and green lines in part b of Figure 9). If the transport through one pathway contains protons hopping, that pathway belongs to the hopping component; otherwise that pathway belongs to the vehicular component. Comparing the distance distribution of the hopping component with that of the vehicular component, the hopping component contains fewer pathways but has a greater average distance. For the second group, which has the longer transport time, the same breakdown shows that most of the transport pathways involve proton hopping (part c of Figure 9). Therefore, the results indicate that the proton hopping mechanism is the dominant mechanism for longer time and distance transport events between sulfonate groups, whereas vehicular motion controls the shorter time and shorter distance transport behavior.

Also noteworthy is the probability of an excess proton transporting to another sulfonate group, that is when a proton leaves the first solvation shell of one sulfonate group, what is the probability of transferring to another sulfonate group instead of coming back? For the system of hydration level 6 at 298 K, the probability of transferring to another sulfonate group is 44.6 ± 8.4% (the error was estimated by bootstrapping technique). When the temperature increases to 340 K, the probability increases to 53.1 ± 6.6%. A similar increase was observed in the other two simulated hydration levels. Therefore, the increase of temperature facilitates PT not only through increasing the proton's overall mobility but also by increasing the probability of transferring to another sulfonate group.

With the increase of the hydration level from 6 to 15, the sulfonate transfer probability decreases to 22.0 ± 3.6% at 298 K. One possible reason is that increasing water concentration leads to a weaker attraction between sulfonate groups and protons, especially when the proton is far from the sulfonate groups. The increase of the average distance between sulfonate groups with increasing hydration also contributes to the decrease in probability. However, this contribution is limited by the small increase in this average distance.

(c). Distribution of Sulfonate Groups and Water Molecules in the PT Pathway. The number of sulfonate groups passed by protons during a specific time period is another essential factor in characterizing the influence of sulfonate groups in the PT. The distribution of the number of distinct sulfonate groups visited by an excess proton during a 1 ns simulation is plotted in Figure 10. The definition of an excess proton visiting a sulfonate group is that an excess proton CEC gets within a distance of 4.3 Angstroms of the sulfonate S atom for a period of at least 0.1 ps. Generally, increasing water content and/or temperature results in more sulfonate groups visited by protons. This indicates that the proton mobility is the main factor controlling the number of sulfonate groups involved in the PT.

The number of water molecules involved in the PT pathways was also analyzed to further characterize the influence of proton hopping on the PT pathway. The water molecules defined as being in the PT pathway are those waters that have a maximum excess proton EVB state amplitude (hydronium-like structure) for at least 0.1 ps. The distribution of water molecule numbers in

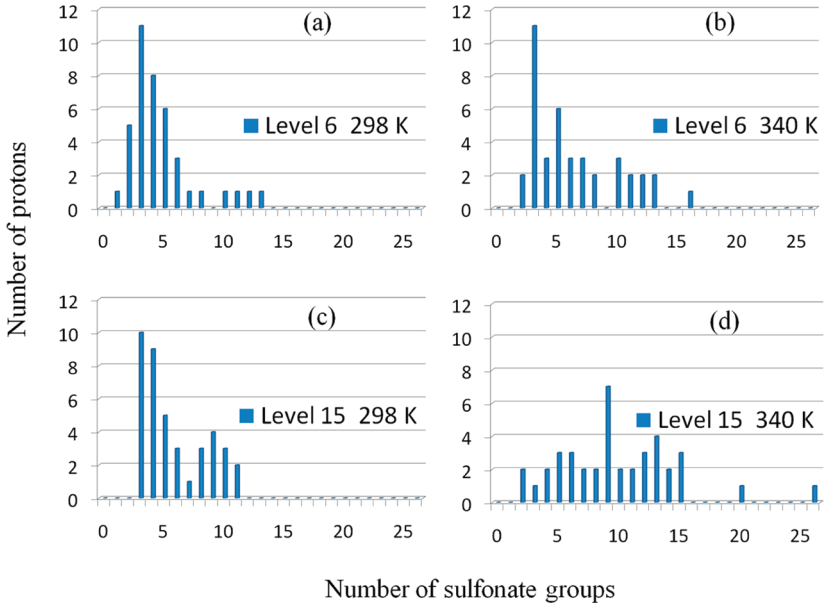

Figure 10. Distribution of the number of sulfonate groups visited by excess protons during 1 ns. The horizontal axis represents the number of sulfonate groups. The vertical axis represents the number of protons. (a) Hydration level 6 at 298 K, (b) hydration level 6 at 340 K, (c) hydration level 15 at 298 K, (d) hydration level 15 at 340 K.

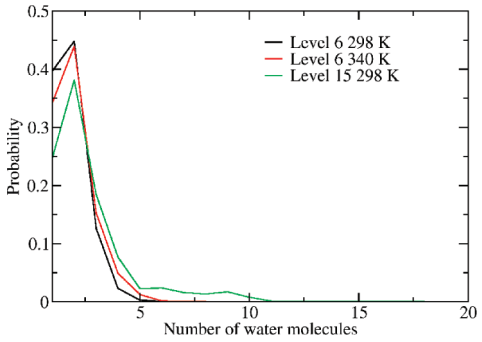

Figure 11. Distribution of the number of water molecule involved in each proton transport pathway. Black line, hydration level 6 at 298 K; red line, hydration level 6 at 340 K; green line, hydration level 15 at 298 K.

the PT pathways is depicted in Figure 11. With an increase of hydration level and temperature, the protons pass more water molecules while transporting from one sulfonate group to another as expected. The peak at 2 water molecules is largely contributed by the Zundel-like cation. The excess proton fluctuates between the 2 water molecules of the Zundel-like cations, leading to the high peak. With the hydration level decreasing from 15 to 6, the increase of the peak reveals that more protons have Zundel-like solvation structures during PT at low hydration levels.

4. CONCLUSIONS

In this work, hydrated Nafion was simulated at different hydration levels and temperatures to investigate the excess proton solvation properties and transport mechanism. The solvation structure was found to be strongly associated with the sulfonate groups. The formation of Zundel- and Eigen-like cations is influenced by their distance to the sulfonate groups. Zundel-like cations are stabilized within the first solvation shell of the sulfonate groups. As the temperature increases, the number of protons in the vicinity of the sulfonate groups also increases. The angle distribution of the proton-related water network shows that the hydrogen bond network involving protons is more stable than the normal water hydrogen bond network. This stability is conserved at the different temperatures and hydration level studied.

The proton diffusion coefficients were estimated from the slope of the excess proton MSDs and the results are in good agreement with experimental measurements at low temperature. The activation energies were estimated from the temperature-dependent diffusion coefficients, and they drop quickly below a hydration level of 10, which agrees with experimental observations. The activation energy at high hydration levels reflects the fact that the proton hopping clearly influences the PT. It was also found that the PT is strongly affected by the hydrophilic domain microstructure.

The PT pathways were analyzed based on the transport distance, proton hopping, the number of sulfonate groups, and the number of water molecules involved. The hopping direction was found to be strongly influenced by the sulfonate groups, especially within the first solvation shell. The PT distance distribution indicates that a majority of the protons will transport to the nearest sulfonate group. Proton hopping was again found to be an important factor during the transport even at the lowest hydration level studied, especially when considering transport times longer than 1.27 ps. When a proton leaves the first coordination shell of a sulfonate group, the probability of transporting to another sulfonate group increases as the temperature increases, and decreases as the water concentration increases. As temperature and water concentration increase, the water distribution shows that the protons visit more water molecules in order to transfer between sulfonate groups. More protons have Zundel-like solvation structures during PT at low hydration levels.

The present simulations demonstrate that the SCI-MS-EVB methodology can accurately describe the physical process of PT

in a PFSA membrane such as Nafion. Such simulation can therefore provide important information for both the understanding and design of new PFSA membranes having additional desirable properties.

AUTHOR INFORMATION

Corresponding Author

*Fax: 773-702-0805, phone: 773-702-7250, e-mail: gavoth@uchicago.edu.

REFERENCES

(1) Li, Q.; He, R.; Jensen, J. O.; Bjerrum, N. J. Approaches and recent development of polymer electrolyte membranes for fuel cells operating above 100 °C. *Chem. Mater.* **2003**, *15*, 4896–4915.

(2) Woo, M. H.; Kwon, O.; Choi, S. H.; Hong, M. Z.; Ha, H.-W.; Kim, K. Zirconium phosphate sulfonated poly (fluorinated arylene ether)s composite membranes for PEMFCs at 100−140 °C. *Electrochim. Acta* **2006**, *51*, 6051–6059.

(3) Heinzel, A.; Barragán, V. M. A review of the state-of-the-art of the methanol crossover in direct methanol fuel cells. *J. Power Sources* **1999**, *84*, 70–74.

(4) Kreuer, K. D. On the development of proton conducting polymer membranes for hydrogen and methanol fuel cells. *J. Membr. Sci.* **2001**, *185*, 29–39.

(5) Costamagna, P.; Yang, C.; Bocarsly, A. B.; Srinivasan, S. Nafion (R) 115/zirconium phosphate composite membranes for operation of PEMFCs above 100 degrees C. *Electrochim. Acta* **2002**, *47*, 1023–1033.

(6) Adjemian, K. T.; Srinivasan, S.; Benziger, J.; Bocarsly, A. B. Investigation of PEMFC operation above 100 degrees C employing perfluorosulfonic acid silicon oxide composite membranes. *J. Power Sources* **2002**, *109*, 356–364.

(7) Choi, P.; Jalani, N. H.; Datta, R. Thermodynamics and proton transport in Nafion - III. Proton transport in Nafion/sulfated ZrO_2 nanocomposite membranes. *J. Electrochem. Soc.* **2005**, *152*, A1548–A1554.

(8) Alberti, G.; Casciola, M.; Massinelli, L.; Bauer, B. Polymeric proton conducting membranes for medium temperature fuel cells (110−160 °C). *J. Membr. Sci.* **2001**, *185*, 73–81.

(9) de Grotthuss, C. J. T. Sur la décomposition de l'eau et des corps qu'elle tient en dissolution à l'aide de l'électricité galvanique. *Ann. Chim. (Cachan, Fr.)*. **1806**, *58*, 54–73.

(10) Agmon, N. The Grotthuss Mechanism. *Chem. Phys. Lett.* **1995**, *244*, 456–462.

(11) Cukierman, S. Et tu, Grotthuss! and other unfinished stories. *Bba-Bioenergetics.* **2006**, *1757*, 876–885.

(12) Tuckerman, M. E.; Chandra, A.; Marx, D. Structure and dynamics of OH-(aq). *Acc. Chem. Res.* **2006**, *39*, 151–158.

(13) Voth, G. A. Computer simulation of proton solvation and transport in aqueous and biomolecular systems. *Acc. Chem. Res.* **2006**, *39*, 143–150.

(14) Wraight, C. A. Chance and design - Proton transfer in water, channels and bioenergetic proteins. *Bba-Bioenergetics.* **2006**, *1757*, 886–912.

(15) Swanson, J. M. J.; Maupin, C. M.; Chen, H. N.; Petersen, M. K.; Xu, J. C.; Wu, Y. J.; Voth, G. A. Proton solvation and transport in aqueous and biomolecular systems: Insights from computer simulations. *J. Phys. Chem. B* **2007**, *111*, 4300–4314.

(16) Ochi, S.; Kamishima, O.; Mizusaki, J.; Kawamura, J. Investigation of proton diffusion in Nafion (R) 117 membrane by electrical conductivity and NMR. *Solid State Ionics* **2009**, *180*, 580–584.

(17) Cappadonia, M.; Erning, J. W.; Niaki, S. M. S.; Stimming, U. Conductance of Nafion 117 membranes as a function of temperature and water content. *Solid State Ionics* **1995**, *77*, 65–69.

(18) D'Epifanio, A.; Navarra, M. A.; Weise, F. C.; Mecheri, B.; Farrington, J.; Licoccia, S.; Greenbaum, S. Composite nafion/sulfated zirconia membranes: Effect of the filler surface properties on proton transport characteristics. *Chem. Mater.* **2010**, *22*, 813–821.

(19) Eikerling, M.; Kornyshev, A. A. Proton transfer in a single pore of a polymer electrolyte membrane. *J. Electroanal. Chem.* **2001**, *502*, 1–14.

(20) Paddison, S. J.; Paul, R. The nature of proton transport in fully hydrated Nafion (R). *Phys. Chem. Chem. Phys.* **2002**, *4*, 1158–1163.

(21) Choi, P.; Jalani, N. H.; Datta, R. Thermodynamics and proton transport in Nafion - II. Proton diffusion mechanisms and conductivity. *J. Electrochem. Soc.* **2005**, *152*, E123–E130.

(22) Petersen, M. K.; Wang, F.; Blake, N. P.; Metiu, H.; Voth, G. A. Excess proton solvation and delocalization in a hydrophilic pocket of the proton conducting polymer membrane narion. *J. Phys. Chem. B* **2005**, *109*, 3727–3730.

(23) Seeliger, D.; Hartnig, C.; Spohr, E. Aqueous pore structure and proton dynamics in solvated Nafion membranes. *Electrochim. Acta* **2005**, *50*, 4234–4240.

(24) Petersen, M. K.; Voth, G. A. Characterization of the solvation and transport of the hydrated proton in the perfluorosulfonic acid membrane nafion. *J. Phys. Chem. B* **2006**, *110*, 18594–18600.

(25) Brandell, D.; Karo, J.; Liivat, A.; Thomas, J. O. Molecular dynamics studies of the Nafion (R), Dow (R) and Aciplex (R) fuel-cell polymer membrane systems. *J. Mol. Model.* **2007**, *13*, 1039–1046.

(26) Elliott, J. A.; Paddison, S. J. Modelling of morphology and proton transport in PFSA membranes. *Phys. Chem. Chem. Phys.* **2007**, *9*, 2602–2618.

(27) Cui, S. T.; Liu, J. W.; Selvan, M. E.; Keffer, D. J.; Edwards, B. J.; Steele, W. V. A molecular dynamics study of a nafion polyelectrolyte membrane and the aqueous phase structure for proton transport. *J. Phys. Chem. B* **2007**, *111*, 2208–2218.

(28) Devanathan, R.; Venkatnathan, A.; Dupuis, M. Atomistic simulation of nafion membrane. 2. Dynamics of water molecules and hydronium ions. *J. Phys. Chem. B* **2007**, *111*, 13006–13013.

(29) Devanathan, R.; Venkatnathan, A.; Dupuis, M. Atomistic simulation of nafion membrane: I. Effect of hydration on membrane nanostructure. *J. Phys. Chem. B.* **2007**, *111*, 8069–8079.

(30) Glezakou, V. A.; Dupuis, M.; Mundy, C. J. Acid/base equilibria in clusters and their role in proton exchange membranes: computational insight. *Phys. Chem. Chem. Phys.* **2007**, *9*, 5752–5760.

(31) Venkatnathan, A.; Devanathan, R.; Dupuis, M. Atomistic simulations of hydrated Nafion and temperature effects on hydronium ion mobility. *J. Phys. Chem. B* **2007**, *111*, 7234–7244.

(32) Choe, Y. K.; Tsuchida, E.; Ikeshoji, T.; Yamakawa, S.; Hyodo, S. Nature of water transport and electro-osmosis in nafion: Insights from first-principles molecular dynamics simulations under an electric field. *J. Phys. Chem. B* **2008**, *112*, 11586–11594.

(33) Cui, S. T.; Liu, J. W.; Selvan, M. E.; Paddison, S. J.; Keffer, D. J.; Edwards, B. J. Comparison of the hydration and diffusion of protons in perfluorosulfonic acid membranes with molecular dynamics simulations. *J. Phys. Chem. B* **2008**, *112*, 13273–13284.

(34) Hristov, I. H.; Paddison, S. J.; Paul, R. Molecular modeling of proton transport in the short-side-chain perfluorosulfonic acid ionomer. *J. Phys. Chem. B* **2008**, *112*, 2937–2949.

(35) Petersen, M. K.; Hatt, A. J.; Voth, G. A. Orientational dynamics of water in the Nafion polymer electrolyte membrane and its relationship to proton transport. *J. Phys. Chem. B* **2008**, *112*, 7754–7761.

(36) Son, D. N.; Kasai, H. Proton transport through aqueous Nafion membrane. *Eur. Phys. J. E: Soft Matter Biol. Phys.* **2009**, *29*, 351–361.

(37) Karo, J.; Aabloo, A.; Thomas, J. O.; Brandell, D. Molecular dynamics modeling of proton transport in nation and hylton nanostructures. *J. Phys. Chem. B* **2010**, *114*, 6056–6064.

(38) Mahajan, C. V.; Ganesan, V. Atomistic simulations of structure of solvated sulfonated poly(ether ether ketone) membranes and their comparisons to Nafion: I. Nanophase segregation and hydrophilic domains. *J. Phys. Chem. B* **2010**, *114*, 8357–8366.

(39) Mahajan, C. V.; Ganesan, V. Atomistic simulations of structure of solvated sulfonated poly(ether ether ketone) membranes and their comparisons to Nafion: II. Structure and transport properties of water, hydronium ions, and methanol. *J. Phys. Chem. B* **2010**, *114*, 8367–8373.

(40) Jang, S. S.; Molinero, V.; Cagin, T.; Goddard, W. A. Nanophase-segregation and transport in Nafion 117 from molecular dynamics simulations: Effect of monomeric sequence. *J. Phys. Chem. B* **2004**, *108*, 3149–3157.
(41) Wescott, J. T.; Qi, Y.; Subramanian, L.; Capehart, T. W. Mesoscale simulation of morphology in hydrated perfluorosulfonic acid membranes. *J. Chem. Phys.* **2006**, *124*, 134702.
(42) Spohr, E. Monte Carlo simulations of a simple lattice model of polymer electrolyte membranes. *J. Mol. Liq.* **2007**, *136*, 288–293.
(43) Knox, C. K.; Voth, G. A. Probing selected morphological models of hydrated nation using large-scale molecular dynamics simulations. *J. Phys. Chem. B* **2010**, *114*, 3205–3218.
(44) Wang, F.; Voth, G. A. A linear-scaling self-consistent generalization of the multistate empirical valence bond method for multiple excess protons in aqueous systems. *J. Chem. Phys.* **2005**, *122*, 144105.
(45) Day, T. J. F.; Soudackov, A. V.; Cuma, M.; Schmitt, U. W.; Voth, G. A. A second generation multistate empirical valence bond model for proton transport in aqueous systems. *J. Chem. Phys.* **2002**, *117*, 5839–5849.
(46) Schmitt, U. W.; Voth, G. A. Multistate empirical valence bond model for proton transport in water. *J. Phys. Chem. B* **1998**, *102*, 5547–5551.
(47) Wu, Y. J.; Chen, H. N.; Wang, F.; Paesani, F.; Voth, G. A. An improved multistate empirical valence bond model for aqueous proton solvation and transport. *J. Phys. Chem. B* **2008**, *112*, 467–482.
(48) Wu, Y. J.; Tepper, H. L.; Voth, G. A. Flexible simple point-charge water model with improved liquid-state properties. *J. Chem. Phys.* **2006**, *124*, 024503.
(49) Spoel, D. v. d.; Lindahl, E.; Hess, B.; Buuren, A. R. V.; Apol, E.; Meulenhoff, P. J.; Tieleman, D. P.; Sijbers, A. L. T. M.; Feenstra, K. A.; Drunen, R. V.; Berendsen, H. J. C. Gromacs User Manual version 4.0. *Gromacs User Manual version 4.0*. 2005.
(50) Agmon, N. Hydrogen bonds, water rotation and proton mobility. *J. Chim. Phys. Phys.-Chim. Biol.* **1996**, *93*, 1714–1736.
(51) Lapid, H.; Agmon, N.; Petersen, M. K.; Voth, G. A. A bond-order analysis of the mechanism for hydrated proton mobility in liquid water. *J. Chem. Phys.* **2005**, *122*, 014506.
(52) Luz, Z.; Meiboom, S. The Activation Energies of Proton Transfer Reactions in Water. *J. Am. Chem. Soc.* **1964**, *86*, 4768–4769.